

Experimental and numerical studies on the seismic performance of RC interior beam-column joints

Meas, Kimreth; Li, Bing; Pham, Thanh Phuong

2014

Meas, K., Li, B., & Pham, T. P. (2014). Experimental and Numerical Studies on the Seismic Performance of RC Interior Beam-Column Joints. *Advances in Structural Engineering*, 17(2), 233-248.

<https://hdl.handle.net/10356/104125>

<https://doi.org/10.1260/1369-4332.17.2.233>

© 2014 Multi-Science Publishing. This paper was published in *Advances in Structural Engineering* and is made available as an electronic reprint (preprint) with permission of Multi-Science Publishing. The paper can be found at the following official DOI: <http://dx.doi.org/10.1260/1369-4332.17.2.233>. One print or electronic copy may be made for personal use only. Systematic or multiple reproduction, distribution to multiple locations via electronic or other means, duplication of any material in this paper for a fee or for commercial purposes, or modification of the content of the paper is prohibited and is subject to penalties under law.

Downloaded on 09 Apr 2024 16:45:16 SGT

Experimental and Numerical Studies on the Seismic Performance of RC Interior Beam-Column Joints

Kimreth Meas, Bing Li* and Thanh Phuong Pham

School of Civil and Environmental Engineering, Nanyang Technological University, Singapore 639798

(Received: 21 August 2012; Received revised form: 19 December 2013; Accepted: 7 January 2014)

Abstract: This paper presents the results from Finite Element (FE) simulation on six Reinforced Concrete (RC) beam-column joints and experimental study. The joints investigate have additional, vertically distributed reinforcement along the beams and lateral cyclic loading is applied, with constant axial force. Experimental results provide insight into the joint behaviour under conventional and unconventional displacement histories in terms of hysteresis loop, crack pattern and joint shear stress. The FE numerical models are validated by comparing the numerical results with experimental results obtained from six tested specimens and two specimens from previous studies. Parametric studies are performed to investigate the complex behaviour of the joints under the influence of axial loads as well as the numbers of vertically distributed reinforcement layers.

Key words: beam-column joint, joint shear stress, drift ratio, column axial load, hysteresis loops, unconventional displacement history.

1. INTRODUCTION

The seismic response of interior reinforced concrete beam-column joints in moment resisting frames has been widely studied since the late 1970s. It has been found that the response of the beam-column joint is influenced by many parameters including: concrete compressive strength, ratio of the total moment capacity of columns to the total moment capacity of beams, joint reinforcement ratio, column axial load ratio, displacement history, etc. Degradation in the region of the joints may result in the loss of lateral load capacity of the frame, compromising the integrity of the frame. Li *et al.* (2002) carried out experiments on two full-scale, non-seismically detailed RC interior beam-wide column joints to investigate the seismic behaviour of the joints under conventional displacement history. From the experimental results, the maximum nominal horizontal shear stress in the joint core was found to be $0.15 f'_c$. The joint without transverse reinforcement failed around the region, at a displacement ductility

factor of 2, which correlates well with the model proposed by Hakuto *et al.* (2000). This suggests that joint shear failure occurs around a displacement ductility factor of 2, where the joint shear stress would lie between $0.11 f'_c$ and $0.17 f'_c$. It should be noted that the modified joint achieved a ductility factor of 3, due to the presence of transverse reinforcement within the joint. Modifying the joint by incorporating heavy transverse reinforcement in the joint region usually leads to construction problems, due to reinforcement congestion and bond control. To improve that condition, Abdel-Fattah and Wight (1987) suggested introducing supplementary intermediate longitudinal reinforcement over a specified length, to move away the potential hinging zone from column face. Abdel-Fattah and Wight (1987) also concluded that placing an intermediate layer of longitudinal reinforcement with an area A_i between 0.3 and 0.35 of the tension reinforcement A_s increases the joint shear resistance. An experimental study conducted by Wong *et al.* (1990)

*Corresponding author. Email address: cbli@ntu.edu.sg; Tel: +65 67905090.

further confirmed that the layers of intermediate reinforcement enhanced the shear capacity of the joint by approximately 7%.

Recently, extensive studies have been carried out to further understand the cyclic response of beam-column joints. Walker (2001) and Alire *et al.* (2002) at University of Washington conducted a series of tests on RC interior beam-column joints without transverse reinforcement at the joint region. Walker *et al.* (2001) used a rich array of displacement histories, including some with highly asymmetric patterns and others with many cycles of constant amplitudes displacement, in addition to the more common symmetric and increasing-amplitude cycles. Alire *et al.* (2002) studied a wide range of joint shear stress demands. It was concluded from the test results that the level of joint shear stress and displacement history had the largest influence on the behaviour of the joint. Although the studies available in past literatures provide information on the seismic behaviours of RC beam-column joints, the effects of several critical factors such as different axial load, vertically distributed longitudinal reinforcement layers, unconventional displacement history with asymmetric cycle pattern are not clearly understood. Therefore, the first part of this paper presents some experimental investigations of two interior RC beam-column joints with limited transverse reinforcement provided in the joint region and four specimens with vertically distributed reinforcement along the beam length; all of which were tested under unconventional and conventional quasi-static load reversal and constant column axial load. In the second part, previous research by Lehman *et al.* (2002) and the tested specimens are used to validate the FE models. Parametric studies are performed to further analyse the seismic joint behaviour under the influence of column axial load and numbers of distributed reinforcement layers.

2. TEST PROGRAM

A total of 6 full-scale specimens of RC interior beam-column joints representing the moment-resisting frame of a building were tested in Protective Engineering laboratory, Nanyang Technological University (NTU), Singapore. The variables in this study consisted of: the ratio of the area of intermediate reinforcement per layer to main tension reinforcement, A_i/A_s , the horizontal displacement history.

2.1. Description of Test Specimens

Specimens were categorised into two different groups, based on the type of applied displacement history. The

three specimens in the first group were tested under conventional displacement history, while the other three in the second group were tested under an unconventional one. The first group specimens were labelled as follows: LS indicates specimens with limited seismic detailing with two transverse reinforcement layers in the joint region, VR3 and VR4 are names for specimens designed with 3 and 4 vertically distributed reinforcement layers along the beam length respectively. The three specimens in the second group (tested under applied unconventional displacement history) were labelled similarly as the first group, along with an additional letter U at the end of specimen. Details of all the specimens are shown in Figure 1.

2.2. Material Properties

For Specimens LS and LSU, deformed bars characterized by yield strength f_y of 520 MPa were used. The average compressive strength of the concrete cylinders on the test day was approximately 43.0 MPa. For Specimens VR3, VR3U, VR4 and VR4U, the deformed bars used for all longitudinal reinforcement were characterized by yield strength f_y of 490 MPa. Plain round bars of 10 mm diameter characterized by yield strength f_y of 370 MPa were used for all link reinforcements. The compressive strength of the concrete cylinders on the test day was about 32.0 MPa on average. The reinforcing steel properties and compressive strength of concrete are shown in Table 1.

2.3. Test Setup

Figure 2 shows a test setup of the specimens tested at NTU, each of which was subjected to a constant axial load and quasi-static load reversals that simulated earthquake loading. The specimens were under quasi-static cyclic loading with displacement control. The bottom of the column was pinned to the floor of the laboratory, while the end of the beam was connected to this floor by steel links, which were restrained against vertical translation but allowed for horizontal translation. A reversible horizontal load was applied to the column using a hydraulic actuator, with a capacity of 50 tons.

For the specimens tested in NTU, two different types of lateral load sequences were applied. As shown in Figure 3, the first lateral load sequences comprised of 3 cycles for each story Drift Ratio (DR); from a DR of 0.25% to 1.0% with 0.25% increment, from 1% to 2% with 0.5 increments then followed by 1.0% increments until the end of the test. This lateral load sequence

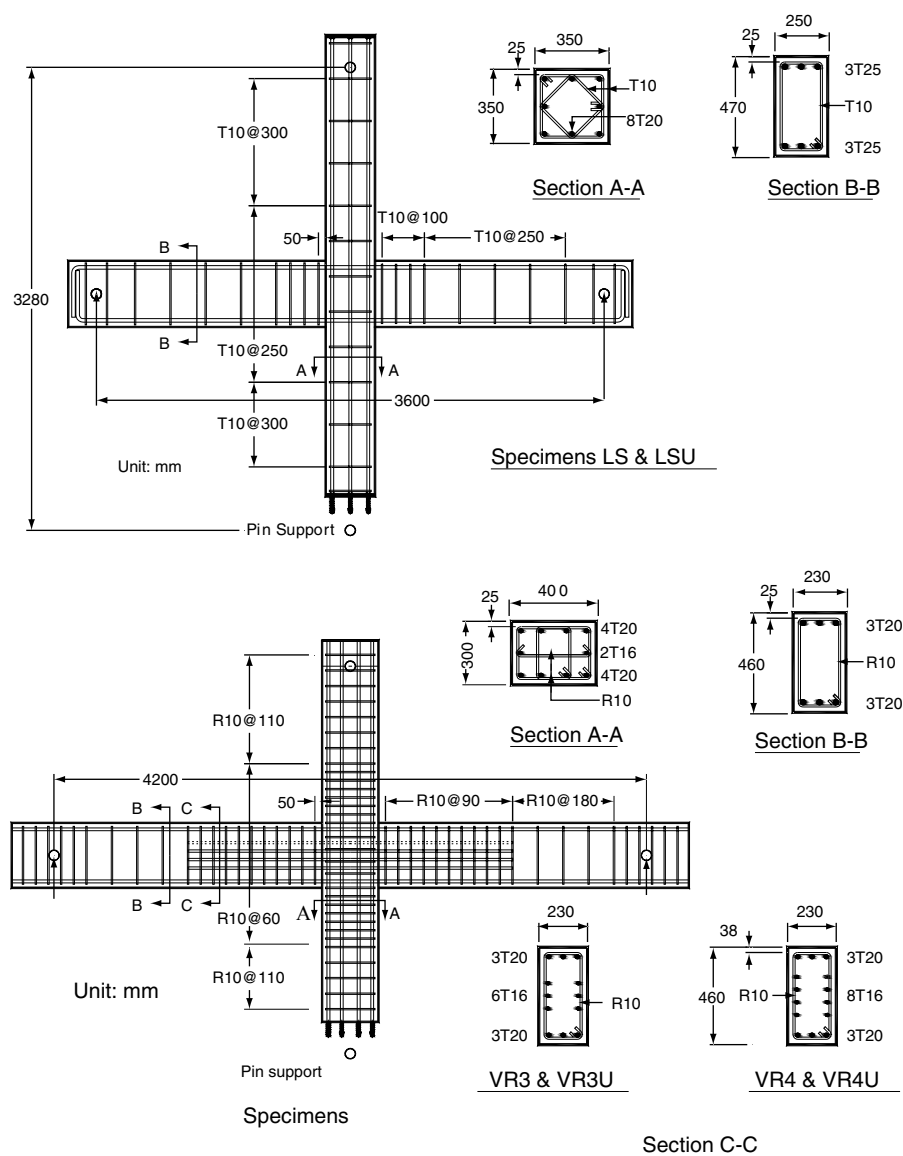


Figure 1. Details of test specimens

Table 1. Material properties

| Specimens | Concrete strength, | Longitudinal reinforcement | | Transverse reinforcement | |
|------------|--------------------|----------------------------|-------------|--------------------------|-------------|
| | f'_c (MPa) | f_y (MPa) | f_u (MPa) | f_y (MPa) | f_u (MPa) |
| LS & LSU | 43.00 | 520.00 | 640.00 | 520.00 | 640.00 |
| VR3 & VR3U | 35.00 | 490.00 | 590.00 | 370.00 | 500.00 |
| VR4 & VR4U | 35.00 | 490.00 | 590.00 | 370.00 | 500.00 |

pattern was used for Specimens LS, VR3 and VR4. The second lateral load sequences, as also shown in Figure 3, consisted of 30 cycles of a story Drift Ratio (DR) of 1.5% then followed by 20 cycles of a DR of 3.0% and lastly followed by two cycles of a DR of 4.0%. This lateral load sequence pattern was used for Specimens

LSU, VR3U and VR4U. It should be noted that Specimens LS and LSU were subjected to lateral load reversals and constant axial loads of $0.15 f'_c A_g$ kN while Specimens VR3, VR3U, VR4 and VR4U were subjected to lateral load reversals and constant axial loads of $0.30 f'_c A_g$ kN.

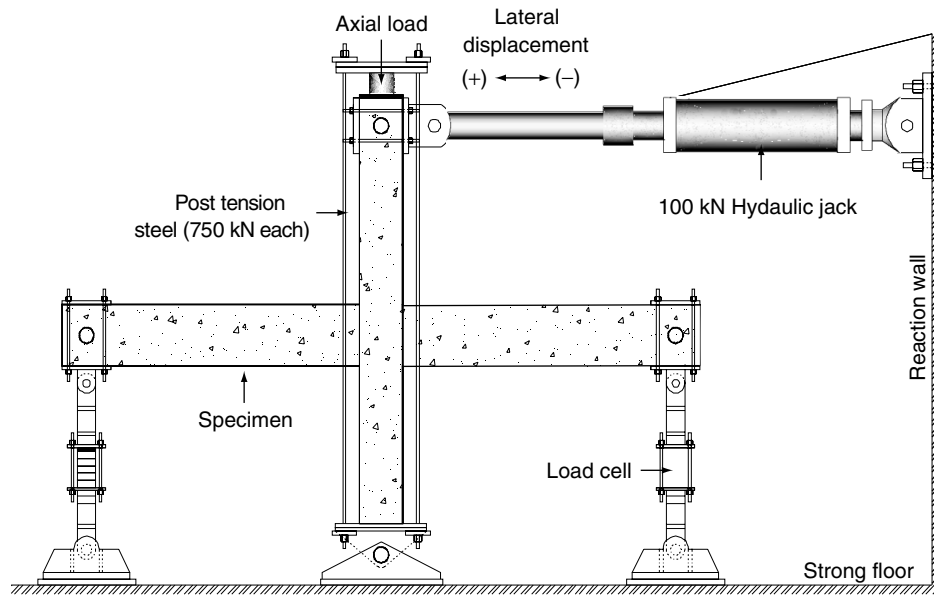


Figure 2. Test setup for specimens

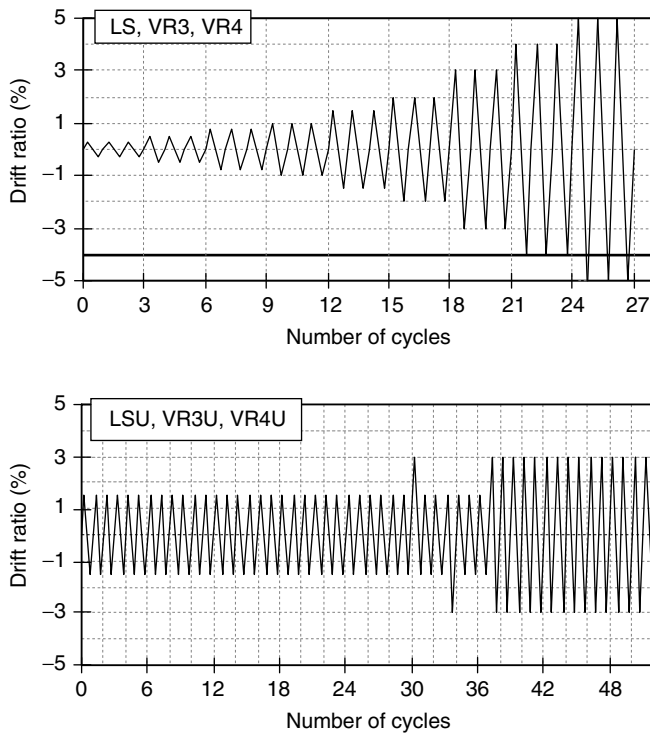


Figure 3. Loading procedures

3. EXPERIMENTAL RESULTS AND OBSERVATIONS

The following sections describe the experimental observations from the tests conducted on all the specimens. In order to determine whether the joint will fail by joint shear or beam flexural failure, the predicted theoretical story shear strength of a beam-column joint is calculated. The predicted theoretical story shear

strength of a beam-column joint is defined as the story shear force at the top of column associated with the theoretical ultimate flexural strength of the beam when a plastic hinge is formed. The predicted theoretical story shear strength of all specimens is shown in Table 2.

3.1. Specimens LS and LSU

Figure 5 illustrates the story shear force versus the horizontal displacement hysteresis loops in continuous line for Specimens LS and LSU. With a limited amount of transverse reinforcement provided in the joint region, both specimens still did not reach their predicted theoretical story shear strength.

For Specimen LS at a DR of $\pm 0.5\%$, more flexural cracks were initiated in the beams than the columns.

In the subsequent loading run to an increased DR of 0.75% , diagonal tension cracks began to appear in the joint region. In the positive loading direction, at a DR of 3.0% , specimen attained a maximum capacity of 146.5 kN , around 43.3% lower than the predicted theoretical story shear strength. At this drift ratio, no yielding was observed on the beam longitudinal reinforcement, but

Table 2. Design parameters of all tested specimens

| Specimens | Joint reinforcement, | | A_i/A_s | $\frac{\sum M_c}{\sum M_b}$ | $P_{th}(\text{kN})$ |
|------------|----------------------|----------------|-----------|-----------------------------|---------------------|
| | $\frac{P}{A_g f'_c}$ | $\rho_{tr} \%$ | | | |
| LS & LSU | 0.15 | 0.50 | 0.00 | 0.87 | 258.60 |
| VR3 & VR3U | 0.30 | 0.97 | 0.43 | 1.02 | 229.51 |
| VR4 & VR4U | 0.30 | 0.97 | 0.43 | 0.95 | 244.81 |

A_i/A_s : The ratio of the area of intermediate reinforcement per layer to main tension reinforcement

the first yield occurred in the column longitudinal reinforcement. This is possibly due to the columns having a lower flexural capacity than the beams. Extensive spalling and crushing of concrete in the joint region was observed at a DR of 3.0%, mainly due to the opening of diagonal cracks and the yielding of the transverse reinforcement in the joint region. At the last tested DR of 4.0%, Specimen LS exhibited a decrease in strength, around 14.0% of its maximum load carrying capacities. The progressive damage and crack pattern of Specimen LS is shown in Figure 4.

Specimen LSU reached a maximum shear capacity of 170.0 kN in the positive loading direction, at a DR of 3.0%. The specimen exhibited a lower horizontal shear capacity than its predicted theoretical story shear strength, by around 34.2% in the positive loading direction. At the first cycle of a DR of 1.5%, the specimen exhibited only one diagonal tension crack in the joint region and a few flexural cracks on the beams. At a DR of 3.0%, the vertical cracks started to occur on the column face on the left and the right sides near the joint region; due to the continuation of the extensive opening of the diagonal cracks in the joint region. Yielding was also observed on the transverse reinforcements in the joint region at this stage. At the last tested DR of 4.0%, LSU exhibited severe strength degradation by around 30.2% of its load carrying capacity. The extensive spalling of concrete at the joint region was observed at this stage, due to the opening of diagonal cracks and the crushing. The progressive damage and crack pattern on this specimen is shown in Figure 5.

Based on the observations, it was concluded that both specimens exhibited joint shear failure without the formation of beam plastic hinges. The maximum joint shear stress, v_{jh} , for Specimen LSU was $0.22 \sqrt{f'_c}$ MPa at a DR of 3.0% which was 13.60% higher than the joint shear stress of Specimen LS, which was $0.19 \sqrt{f'_c}$ MPa at a DR of 3.0%. The joint shear stress versus drift ratio envelope curve is shown in Figure 6 for both specimens. From this curve, it was also concluded that unconventional displacement history influenced the seismic behaviour of the specimen, by increasing the joint shear stress.

3.2. Specimens VR3 and VR3U

The story shear force versus horizontal displacement hysteresis loop of Specimen VR3 is shown in Figure 4. This specimen also did not reach its theoretical story shear force during testing. The specimen showed a significant pinching behaviour throughout the test. Fine flexural cracks were initiated and spread along the

beams during the elastic loading cycles up to a DR of 1.0%. The specimen developed some diagonal tension cracks within the joint core at a DR of 1.0%. In the subsequent inelastic loading cycle range, there was an intensive formation of diagonal tension cracks within the joint core. The specimen attained its maximum capacities of approximately 175.0 kN, in the positive loading direction and 156.2 kN, in the negative loading direction corresponding to a DR of 3.0%. This specimen exhibited a lower horizontal shear capacity by around 22.66% in the positive loading direction than its predicted theoretical story shear force, for when a plastic hinge develops in the beam. Flexural cracks also appeared on the bottom column in the regions close to the joint. At a DR of 4.0%, crushing of diagonal compression struts and spalling of concrete at the joint core due to the opening of diagonal tension cracks were observed. The crack pattern of Specimen VR3 at the end of the test is shown in Figure 5.

The story shear force versus the horizontal displacement hysteresis loop for Specimen VR3U under unconventional displacement history is shown in Figure 4. For the first cycle of story drift ratio of 1.5%, beam flexural cracks and joint cracks were observed, while fewer flexural cracks were observed on the columns than on the beams and the joint region. The maximum shear capacity attained was approximately 206.3 kN at a DR of 3.0% in positive loading direction. Specimen VR3U exhibited strength degradation by 8.8% in positive loading direction as compared to its predicted theoretical story shear strength. In the subsequent loading run, during the first cycle of a DR of 3.0%, the specimen exhibited more diagonal tension cracks in the joint region. In the further ahead, in the 15th cycle of a DR of 3.0%, the diagonal cracks in the joint region propagated extensively, resulting in wider crack width and spalling of concrete cover at the joint region. At the last drift ratio of 4.0%, Specimen VR3U exhibited strength degradation by around 29.0% and showed severe spalling of the concrete cover of the joint region, which was around 80% of the joint area. The crack pattern of Specimen VR3 at the end of the test is shown in Figure 5. Therefore, it can be expected that the diagonal concrete compression strut failure might have dominated the failure mechanism of the joint.

The maximum joint shear stress, v_{jh} for Specimen VR3U was $0.30 \sqrt{f'_c}$ MPa at a DR of 3.0%, which was 20.67% higher than the joint shear stress of Specimen VR3, which was $0.25 \sqrt{f'_c}$ MPa at a DR of 3.0%. The comparison of joint shear stress versus drift ratio envelope curves for both specimens is shown in Figure 6. It was also concluded from this curve that

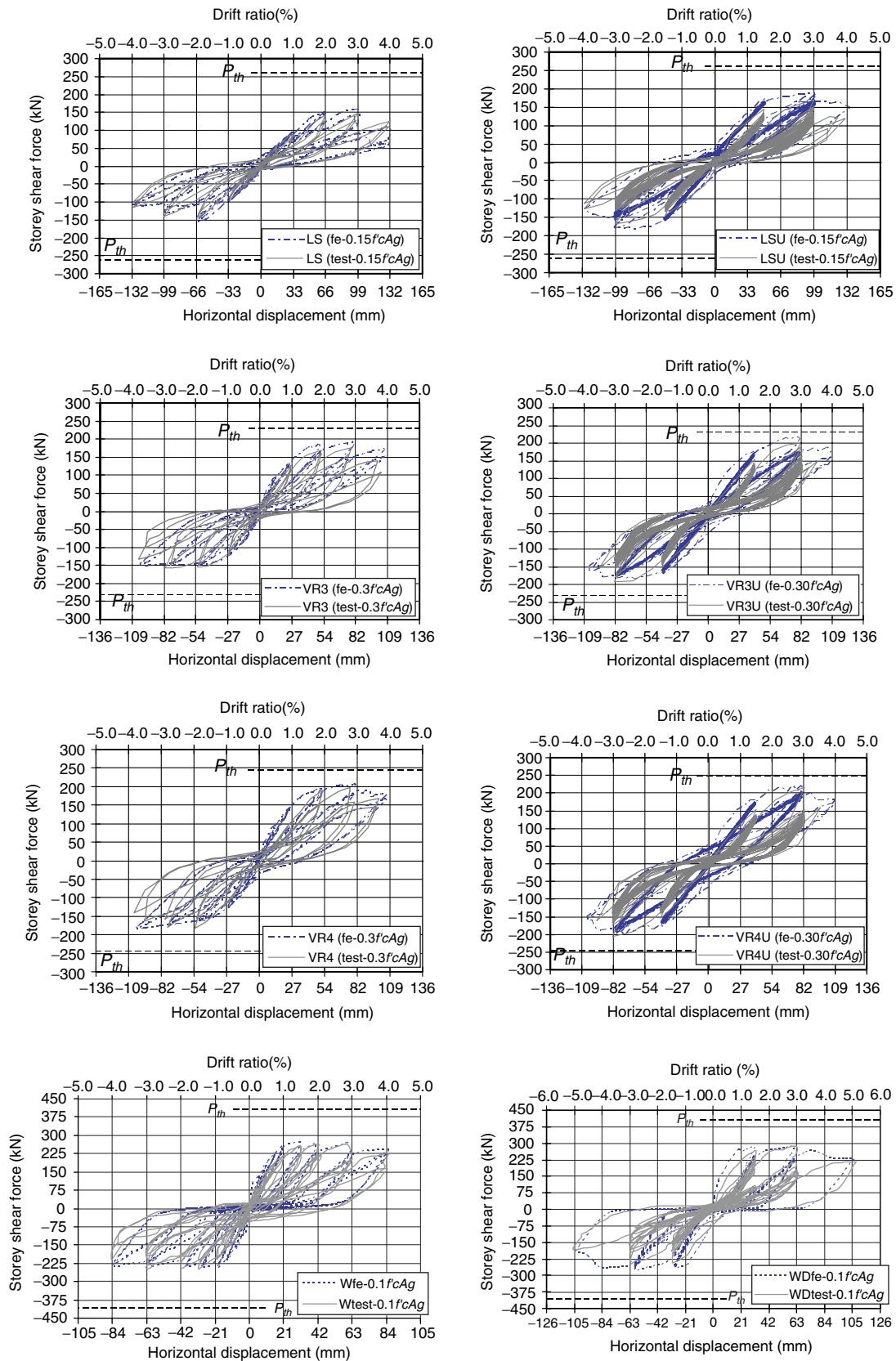


Figure 4. Story shear versus story displacement hysteresis loops

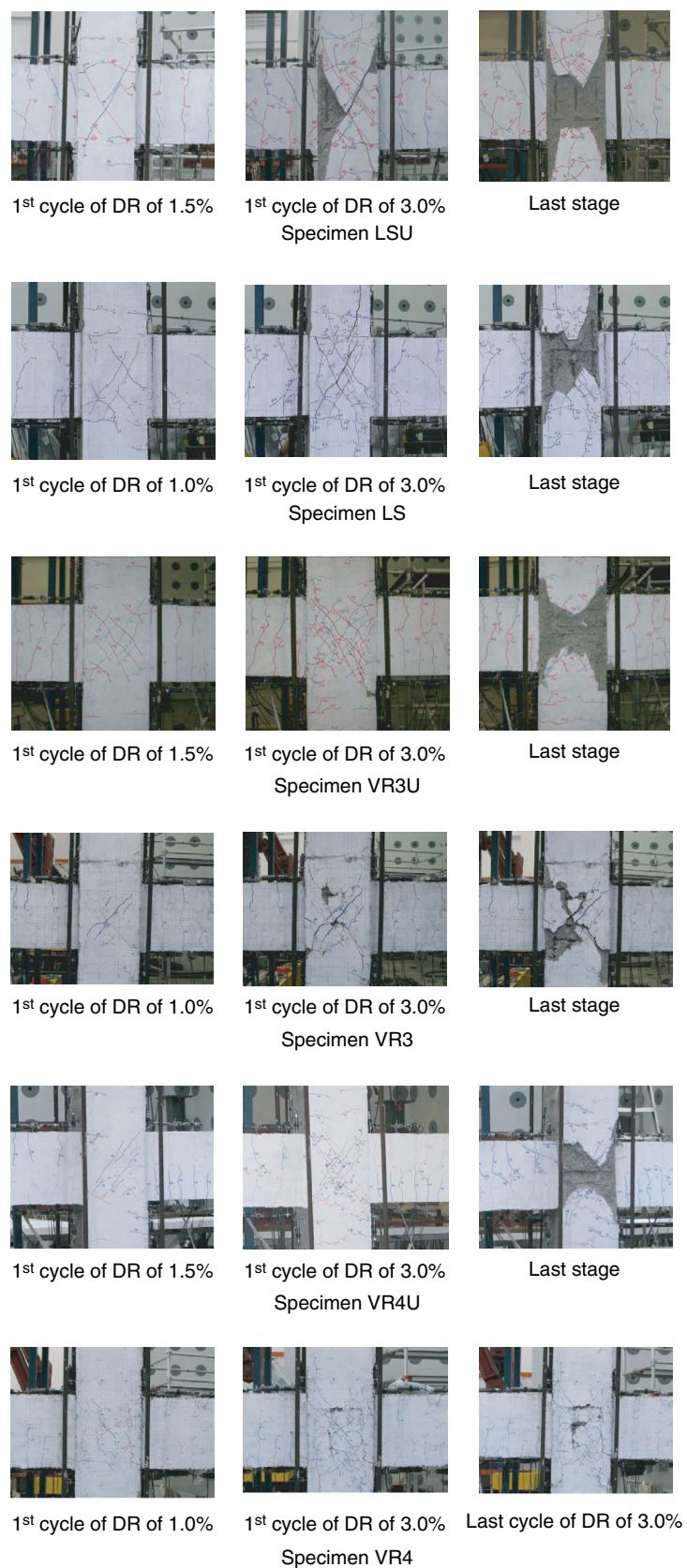


Figure 5. Observed crack patterns

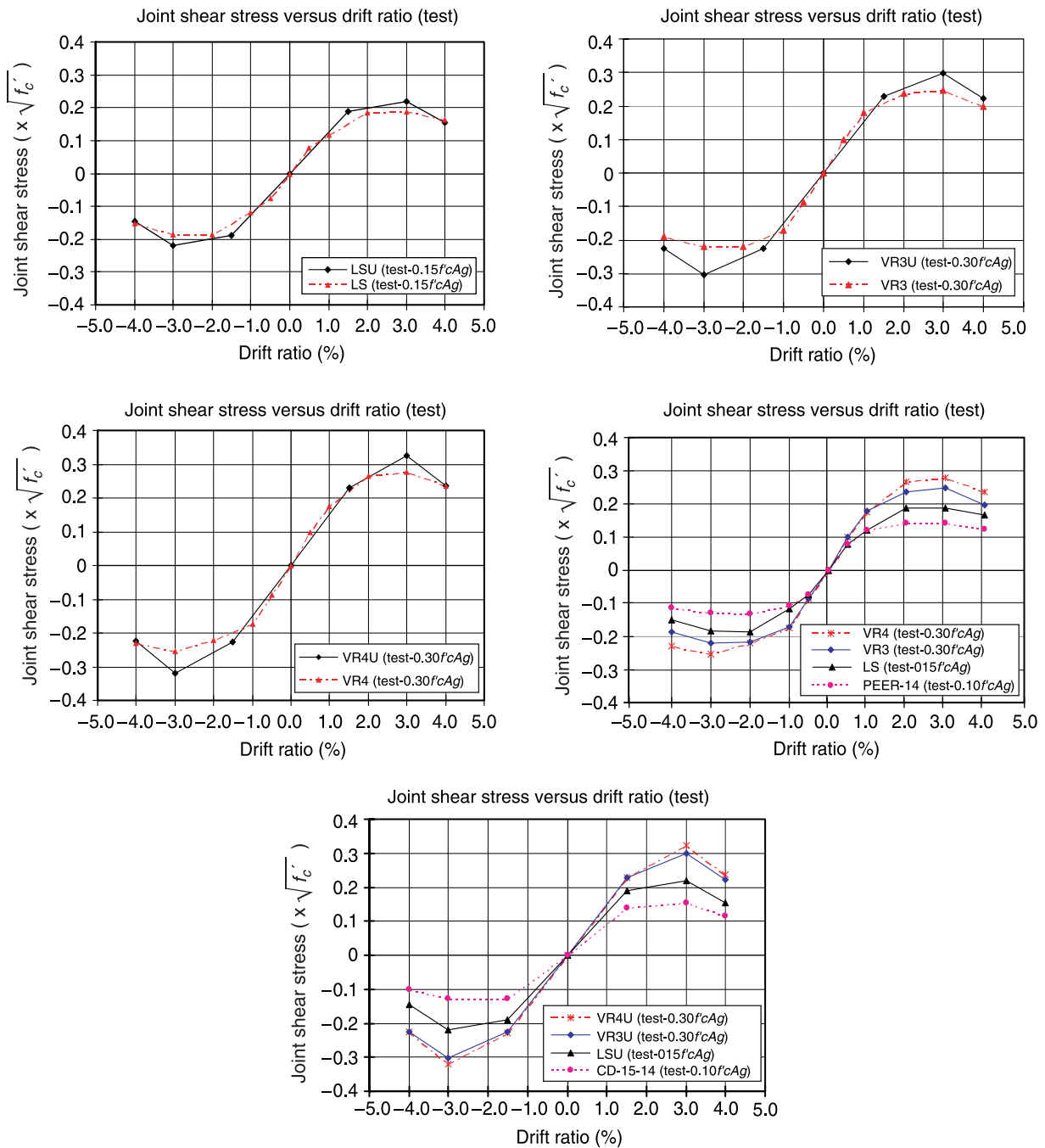


Figure 6. Joint shear stress versus drift ratio comparison

unconventional displacement history influenced the seismic behaviour of the specimen, by increasing the joint shear stress.

3.3. Specimens VR4 and VR4U

The story shear force versus horizontal displacement hysteresis loop for Specimen VR4 is shown in Figure 4. The maximum shear capacities of 197.0 kN in the positive and 180.8 kN in the negative loading directions were reached at a DR of 3.0%. This specimen exhibited a

lower horizontal shear capacity by about 19.50% in the positive loading direction than its predicted theoretical story shear strength. At a DR of 2.0%, Specimen VR4 experienced stiffness degradation and a significant pinching behaviour after the second loading cycle. At a DR of 4.0%, the specimen experienced a substantial loss by more than 20% of its load carrying capacity, which led to the test being stopped. The progressive damage and cracking pattern exhibited by Specimen VR4 was quite analogous to Specimen VR3 and is shown in Figure 5.

The story shear force versus the horizontal displacement hysteresis loop for Specimen VR4U under unconventional displacement history is depicted in Figure 5. The maximum shear strength attained was approximately 214.0 kN at a DR of 3.0% in positive loading directions. VR4U exhibited lower shear strength by 12.6% in positive loading direction than its predicted theoretical story shear strength. The progressive damage and cracking pattern exhibited by Specimen VR4U was quite analogous to Specimen VR3U throughout the test and is shown in Figure 6. At the last applied DR of 4.0%, VR4U exhibited strength degradation by around 26.2%, respectively and showed severe spalling of the concrete cover of the joint region.

The maximum joint shear stress, v_{jh} for Specimen VR4U was $0.32 \sqrt{f'_c}$ MPa at a DR of 3.0%, which was 14.3% higher than joint shear stress of Specimen VR4, which was $0.28 \sqrt{f'_c}$ MPa at a DR of 3.0%. The comparison of joint shear stress versus drift ratio envelope curve for both specimens is shown in Figure 6. It can also be concluded from this curve the unconventional displacement history tends to increase the maximum joint shear stress.

3.4. Specimens Tested under Conventional Displacement History

It was of interest to compare the joint shear stress with drift ratio envelope curves of all specimens under conventional displacement history. The comparisons are shown in Figure 6. Specimen LS with limited seismic detailing reached maximum joint shear stress, v_{jh} , of $0.19 \sqrt{f'_c}$ MPa at a DR of 3.0%. When placing an additional three or four vertical reinforcing bars to the joint region in specimen LS, its joint shear strength appeared to increase by 31.57% (in specimen VR3) and 47.36% (in specimen VR4), respectively.

3.5. Specimens Tested under Unconventional Displacement History

The comparison of the joint shear stress versus drift ratio envelope curves of all specimens under unconventional displacement history, LSU, VR3U and VR4U, is shown in Figure 7. Specimen LSU with limited seismic detailing reached maximum joint shear stress of $0.22 \sqrt{f'_c}$ MPa at drift ratio of 3.0%. Under unconventional displacement history, placing additional three or four vertical reinforcing bars to the joint region of LSU resulted in an increase of maximum joint shear stress by 36.36% (in specimen VR3U) and 45.45% (in specimen VR4U), respectively.

The above comparisons (sections 3.4 and 3.5) highlighted that the loading history and additional

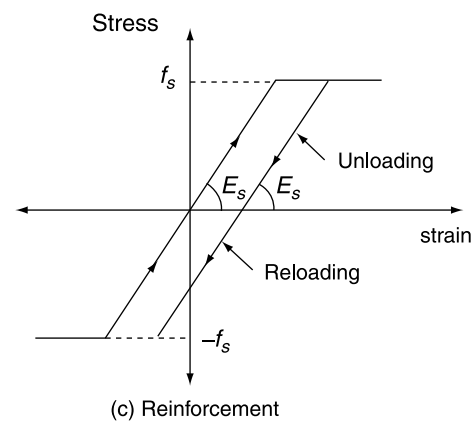
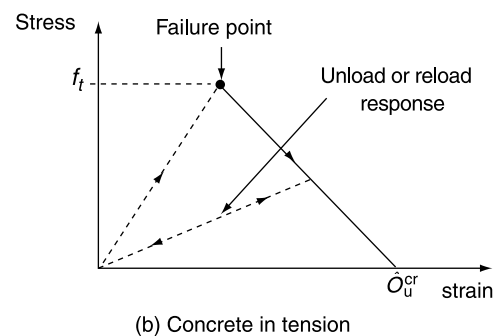
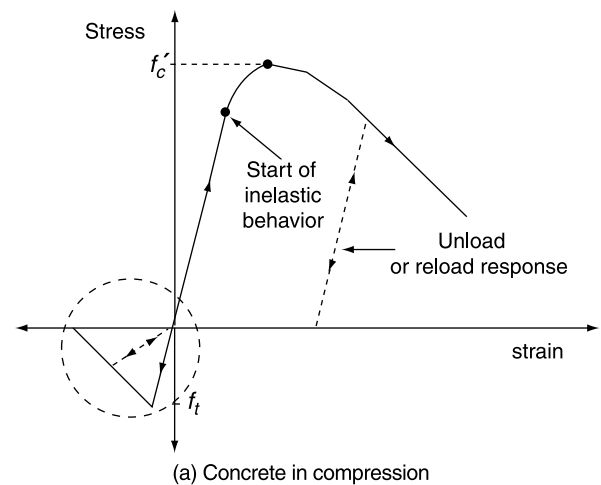


Figure 7. Material modeling

vertical reinforcement do not affect to the drift ratio at maximum shear force.

4. FINITE ELEMENT ANALYSIS

It is possible to thoroughly evaluate the stresses and deformations in a structure using FE analysis, rather than carrying out an experimental study. The nonlinear FE analysis can give a better understanding of the mechanical behavior of a structure. The present study uses the DIANA software (2000) in the analysis. Two-dimensional (2D) plane stress elements were applied to simulate the concrete, while reinforcing bars were

modelled as truss elements. The following sections present the finite element study carried out to validate the models and perform critical parametric investigations.

4.1. Modelling of Concrete

The analysis uses a constant stress cut-off criterion for the cracking of concrete, as presented by Hajime and Kohichi (1991). According to this model, a crack is assumed to be initiated perpendicular to the major principal stress if its value exceeds the tensile strength and is independent of other principal stresses. The orientation of the crack is then stored and the material's response perpendicular to the crack is determined by a stress-strain relationship for the cracked material volume. Additional cracks may appear at the same location, but their formation to the existing cracks is greater than 15° . However, if the angle is less than that, the secondary cracks are assumed not to have been generated, even when the tensile stress has reached its fracture envelope.

The fracture energy G_F and the tensile strength f_t of the concrete were used to calculate the value of ultimate crack opening w_u . G_F of the concrete was calculated

using a three-point bending test based upon the recommendations of RILEM 50-FMC (1985). To simulate the softening effect of the concrete in tension after cracking, a bilinear tension stress-strain curve was used as shown in Figure 8(b) in which ϵ_u^{cr} was taken as 0.001. The value was based on the assumption that the strain softening after failure reduces the stress linearly to zero at a total strain of about 10 times the strain at failure of concrete in tension, which is typically 0.0001. The uniaxial tensile strength of concrete f_t used in the analysis was determined from the compressive strength f_c according to the CEB-FIP Model code (1990):

$$f_t = 0.30(f_c)^{2/3} \quad (1)$$

When the cracked concrete is unloaded in tension, the secant modulus is used to evaluate the stiffness, owing to the fact that the strain across the crack is linearly reduced to zero as the stress approaches zero as shown in Figure 7(b). However, when the concrete in compression is unloaded, the initial stiffness is adopted for the stiffness calculations as shown in Figure 7(a).

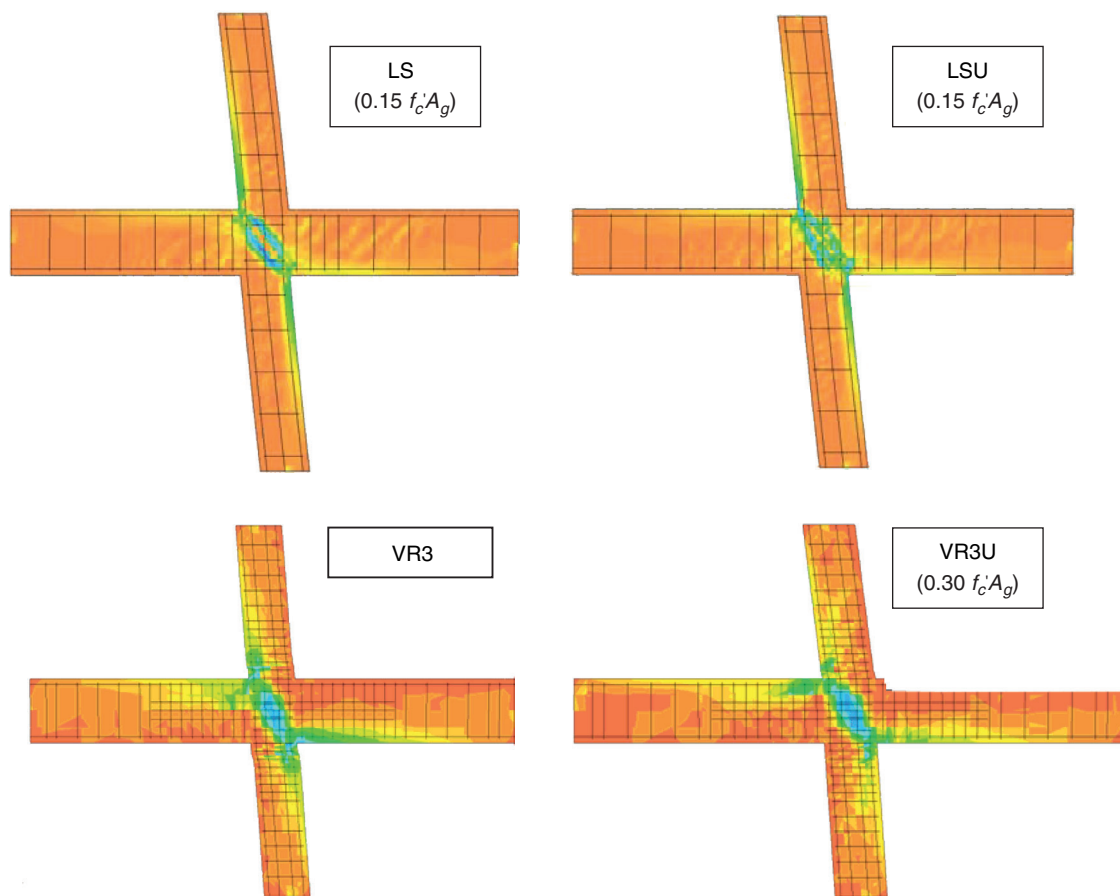


Figure 8. Major stress distribution of FE model in deformed shape

The response of the concrete in compression was taken into account by an elastic-plastic model. The elastic state of stress was limited by a Drucker-Prager yield surface. Isotropic hardening with an associated flow rule was used after yielding of the surface had occurred. The DIANA software evaluates the yield surface using the current state of stress, the angle of internal friction ϕ , and the cohesion c . As per the recommendations of the DIANA software manual, the angle of internal friction in concrete can be approximated to be 30° . The cohesion c used in the analysis is given by formula as follows:

$$c = f_c \left(\varepsilon_{uniaxial}^p \right) \frac{1 - \sin \phi}{2 \cos \phi} \quad (2)$$

where $f_c \left(\varepsilon_{uniaxial}^p \right)$ is the hardening or softening parameter as a function of the plastic strain in the direction of the uniaxial compression stress. Standard uniaxial tests on concrete cylinders were used to define the stress-strain relations up to the peak stress. CEB-FIP recommendations can be used to evaluate the post-peak behavior of the concrete using cylinder compression strength tests. A Poisson's ratio of 0.15 was used in the analysis.

4.2. Modelling of Reinforcement

A uniaxial bi-linear stress-strain relationship without strain hardening was used to describe the constitutive behavior of the reinforcement. The bars were modelled with the DIANA options of separate truss elements. During the test, bond deterioration along the beam's longitudinal bars and column main bars, particularly in joint region, were found and necessary slippage of the steel bars was expected to occur. Bond-slip models with the DIANA options were accounted between the reinforcement and surrounding concrete. Figure 7(c) defines the stress-strain relationship for the reinforcing steel, which was modelled with an elasto-plastic curve.

4.3. Verification of Finite Element Model

The analytical results were compared with those obtained from the experiments on the 6 specimens carried out in NTU and two specimens PEER-14 and CD-15-14 obtained from a report by Lehman *et al.* (2002) to verify the finite element model. Specimens PEER-14 and CD-15-14 were non-ductile without transverse reinforcement in the joint core. The concrete was modelled using eight-noded iso-parametric 2D plane stress elements and the reinforcing steel bars were modelled as two-noded truss elements. The constant axial load on the top of the column was applied as a

distributed loading while the horizontal cyclic load was applied on to a central node on the model.

4.3.1. Load-displacement responses of specimens

Figure 4 shows the predicted and observed load-displacement responses of all specimens. The hysteresis loop of analytical models and all tested specimens display the accuracy of the analytical model.

For Specimen LS, as observed from Figure 4, the FE model achieved higher maximum story shear force by around 7.3% than the tested specimen at the same DR of about 3.0%. The story shear force of the last cycle of the analytical results was slightly lower. For Specimen LSU also shown in Figure 4, the analytical result showed a higher shear capacity by around 9.9% than its experimental counterpart at maximum capacity in the positive loading cycle of a DR of 3.0%. FE result has shown similar pinching behaviour to the tested specimen.

For response of Specimen VR3, as seen from Figure 4, the analytical model reached higher maximum a shear capacity by 9.7% than the tested specimen at the same DR of 3.0%. Pinching behaviour was analogous to that of the tested specimen. For the response of Specimen VR3U as shown in Figure 4, the overall correlation of story shear forces observed between the experimental and analytical results was fairly good. The analytical model reached a higher maximum shear capacity by around 7.3% than the tested specimen at the same DR of 3.0% in positive loading cycle.

For Specimen VR4, as seen from Figure 4, the analytical model reached almost the same maximum shear capacity at the same DR of 3.0% as that of the tested specimen. Pinching behavior observed was similar to that in the tested specimen. For Specimen VR3U, as shown in Figure 4, the maximum story shear force observed between the experimental and analytical results was almost the same at a drift ratio of 3.0%. However, the pinching behavior of the analytical model was a bit fatter than the experimental one.

For Specimen PEER-14, as observed from Figure 4, the FE model achieved almost the same maximum shear capacity at the same DR of about 2.0% as that of the tested specimen. The pinching behavior of the analytical result was a bit smaller than experimental one. For Specimen CD-15-14 as shown in Figure 4, the predicted response correlated well with its experimental counterpart.

The major principal stress distribution within the Specimens LS, LSU, VR3 and VR3U with deformed shapes is also seen in Figure 8. Although the intensity of the strains and their distribution varied for different

DRs, their major concentration in and around the joint was particularly noticeable for both Specimens PEER-14 and CD-15-14. Larger stress concentrations extended to the upper and lower parts of the columns and the left and the right sections of the beams for the specimens enhanced with reinforcement and vertically distributed reinforcement in the joint region. These showed the significant contribution of flexural deformation of beam and column to the total deformation; apart from the joint shear deformation. Comparison of the analytical and experimental results of all specimens showed that the lateral load-displacement hysteresis loops obtained from the FE analyses were quite similar to the experimental observations. From the aforementioned observations and predictions of the global behaviour using the FE analysis, the use of FE modelling techniques can, therefore, be further extended to study the joint performance, by varying different parameters.

4.4. Parametric Studies

The level of applied axial load influences the behaviours of non-ductile and ductile RC beam-column joints and it remains inconclusive of what is the maximum level of this applied constant axial force that affects the behavior. Moreover, the effects of vertically distributed reinforcement layers used to enhance joint shear, were too complex to be predicted either with the experimental observations of the tested specimens or with the investigations available in literature. The following sections present the application of the FE modelling technique to investigate the critical influencing parameters such as the axial load and numbers of vertically distributed layers.

4.4.1. Influence of axial loads on the behavior of beam-column joints

Analytical research studies have proved that axial loading is a critical parameter in the studies of beam-column joints; however, its effect on seismic behavior of beam-column joints has not been fully understood. In addition, past investigations have shown that axial force up to a certain level was beneficial to the joint shear resistance as reported by Li *et al.* (2003). In an experimental study conducted by Fu *et al.* (2000), it was pointed out that if the joint shear was small, an increase of axial loads was favourable to the joints, while in contrast for high joint shears, an increase of axial loads was unfavourable. Li *et al.* (2003) found that for an oblong joint, an axial load from zero to $0.4 f'_c A_g$ was beneficial to the joint, while the axial compression load ranging between 0 to $0.2 f'_c A_g$

enhanced the joint's performance for deep wall-like column joints.

In this study, the influence of axial loading on non-ductile and moderate ductile RC beam-column joints subjected to seismic loading was investigated. The same horizontal loading histories as those used in the experiments were applied. Figure 9 showed the envelopes of the analytical hysteretic responses corresponding to different axial load levels of all specimens. The applied axial load was varied from 0 to $f'_c A_g$.

From Figure 9, it was seen that Specimens LS and LSU, designed with limited ductile joint, attained an optimum value of ultimate story with an enhancement of around 11.4% and 12.0%, respectively in story shear forces when axial load ratio was $N^*/A_g f'_c = 0.3$ as compared to when axial load ratio was zero. A slight reduction of story shear force was observed at an axial load ratio of 0.45 when compared with an axial load ratio of 0.3. A further increase in axial load decreased the story shear forces.

For the joints with limited seismic detailing, VR3 and VR3U attained an optimum value of ultimate story force with an enhancement of around 12.5% and 12.7%, respectively in story shears when axial load ratio was $N^*/A_g f'_c = 0.3$ as compared to when axial load ratio was zero. A slight reduction of story shear force was observed at an axial load ratio of 0.45 when compared with an axial load ratio of 0.3. A similar trend presented itself with VR4 and VR4U, which attained an optimum value of ultimate story, shear strength with an enhancement by around 12.8% and 13.0%, respectively in story shear forces when axial load ratio was $N^*/A_g f'_c = 0.3$ as compared to when axial load ratio was $N^*/A_g f'_c = 0.0$. A slight reduction of story shear was observed at an axial load ratio of 0.45 when compared with an axial load ratio of 0.3.

However, the analytical result showed that non-ductile Specimens PEER -14 and CD-15-14 attained an optimum value of ultimate story shear strength with an enhancement of around 10.0% and 11.2%, respectively in story shear forces when axial load ratio was $N^*/A_g f'_c = 0.15$ as compared to when axial load ratio was $N^*/A_g f'_c = 0.0$. A slight reduction of story shear was observed at an axial load ratio of 0.30 when compared with an axial load ratio of 0.15. It may be concluded that an axial load ratio of $N^*/A_g f'_c \leq 0.15$ is beneficial to the joint's performance and a further increase in axial load ratio would prove to be detrimental, as it adversely affects the story shear strength of non-ductile joints.

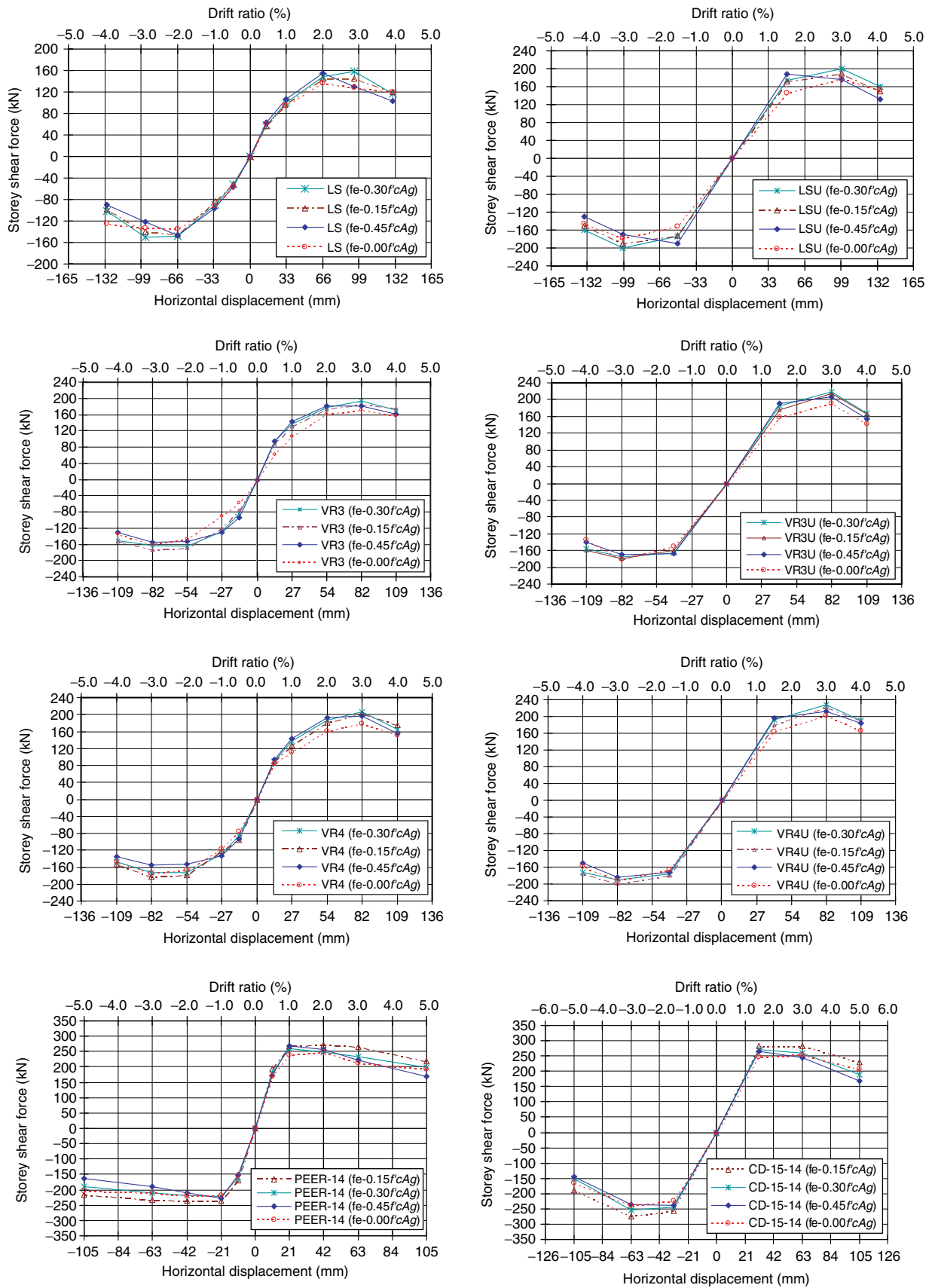


Figure 9. Joint performance of FE model under axial load

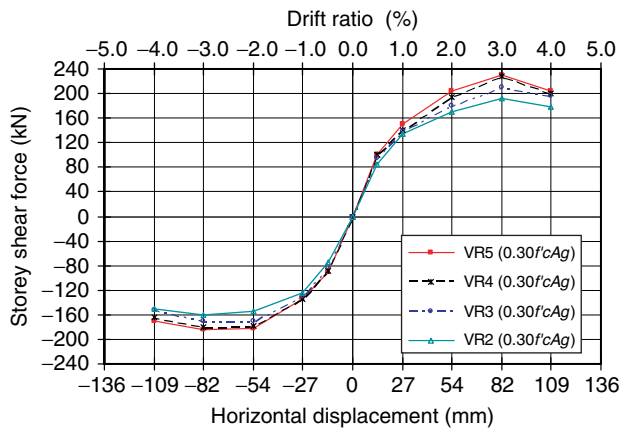


Figure 10. Influence of numbers of distributed reinforcement layers

4.4.2. Influence of vertically distributed reinforcement layers on joint behavior

The experimental investigations of Specimens VR3 and VR4 under conventional displacement history showed that Specimen VR4, enhanced with 4 vertically distributed reinforcement layers, exhibited a significant improvement in shear strength by around 12.5% higher than Specimen VR3, enhanced with 3 vertically distributed reinforcement layers. One distributed reinforcement layer contained two bars having a total area of 402 mm²; one on each beam face. Figure 9 showed the comparison of the envelopes of the analytical hysteretic responses of the models enhanced with 2, 3, 4, and 5 vertically distributed reinforcement layers in the joints. As seen in Figure 10, the results show that the model enhanced with 3 layers had a higher shear by around 8.3% than the one enhanced with 2 layers and the model enhanced with 4 layers had a higher shear by around 9.1% than that enhanced with 3 layers. However, it seems that the model enhanced with 5 layers had little increase of story shear strength, by around 1.5% higher, than the one with 4 layers. Therefore, it can be concluded that placing additional vertically distributed reinforcement layers can provide a significant improvement in joint shear strength. The shear strength enhancement was 18.9% for the cases with two to four layers placed. However, placing more than four layers did not further improve the response of the joints.

5. CONCLUSIONS

The seismic behaviours of the reinforcement beam-column joints were investigated using the experimental and analytical studies. Six full-scale interior beam-column joints, with or without additional longitudinal layers in the beam, were

constructed and tested under conventional or unconventional loading history. An FE analysis was employed as a numerical tool to further investigate the performance of the joints. The results obtained from the numerical study were compared with experimental results, and was shown to be reliable. The predicted results matched well with the experimental observations. Based on the experimental and finite element numerical study results, the following conclusions can be drawn:

- (1) Additional longitudinal reinforcement layers in the beam significantly increase joint shear strength. Placing additional three or four layers could result in an increment in maximum joint shear stress of 31-36% and 45-47%, respectively. No significant effect of loading history in terms of joint shear strength increment. The loading history and additional vertical reinforcing bars do not significantly affect the drift ratio at maximum shear force.
- (2) For the joints with limited seismic detailing, Specimen tested under unconventional displacement history (LSU) produced 13.6% higher joint shear stress strength than that of Specimen tested under conventional displacement history (LU). FE analytical results showed that the maximum level of axial load ratio $N^*/A_g f'_c \leq 0.30$ was beneficial to joint response under both conventional and unconventional displacement histories.
- (3) For the joints with vertically distributed reinforcement detailing, the maximum joint shear stress rose by roughly 15% in specimens tested under unconventional displacement history (VR3U and VR4U) comparing to those tested under conventional conditions (VR3 and VR4). FE analytical results showed that the maximum level of axial load ratio $N^*/A_g f'_c \leq 0.30$ was beneficial to joint response under both unconventional and conventional displacement histories.
- (4) The experimental joint shear stress of Specimens PEER-14 and CD-15-14 without transverse reinforcement in the joint core was observed to be around $0.17 \sqrt{f'_c}$ MPa as reported in the PEER report by Lehman *et al.* (2002). FE analytical results showed that the maximum level of axial load ratio of $N^*/A_g f'_c \leq 0.15$ was beneficial to joint response under both unconventional and conventional displacement histories.

REFERENCES

- Abdel-Fattah, B. and Wight, J.K. (1987). "Study of moving beam hinging zones for earthquake-resistant design of R/C buildings", *ACI Structural Journal*, Vol. 84, No. 1, pp. 31–39.
- Alire, D.A. (2002). *Seismic Evaluation of Existing Unconfined Reinforced Concrete Beam–Column Joints*, Master Thesis, Department of Civil and Environmental Engineering, University of Washington, Washington D.C., USA.
- CEB-FIP (1990). *CEB-FIP Model Code: Design Code*, Thomas Telford, Lausanne, Switzerland.
- DIANA (2000). *DIANA User's Manual: Finite Element Analysis User's Manual-Nonlinear Analysis*, Version 7, TNO Building and Construction Research, Delft, The Netherlands.
- Fu, J., Chen, T., Wang, Z. and Bai, S. (2000). "Effect of axial load ratio on seismic behavior of interior beam-column joints", *Proceedings of the 12th World Conference on Earthquake Engineering (12WCEE)*, Auckland, New Zealand.
- Li, B., Wu, Y.M. and Pan, T.C. (2002). "Seismic behavior of non-seismically detailed interior beam-wide column joints-Part I: Experimental results and observed behavior," *ACI Structural Journal*, Vol. 99, No. 6, pp. 791–802.
- Li, B., Wu, Y. and Pan, T.C. (2003). "Seismic behavior of nonseismically detailed interior beam-wide column joints-Part II: Theoretical comparisons and analytical studies", *ACI Structural Journal*, Vol. 100, No.1, pp. 56–65.
- Li, B., Tran, C.T.N. and Pan, T.C. (2009). "Experimental and numerical investigations on the seismic performance of lightly reinforced concrete joints", *Journal of Structural Engineering*, ASCE, Vol. 135 No.9, pp. 1007–1018.
- Li, B. and Tran C.T.N. (2009). "Seismic behaviour of reinforced concrete beam-column joints with vertical distributed reinforcement", *ACI Structural Journal*, Vol. 106, No.6, pp. 790–799.
- Okamura, H. and Maekawa, K. (1991). *Nonlinear Analysis and Constitutive Models of Reinforced Concrete*, Gihodo, Tokyo, Japan.
- Hakuto, S., Park, R. and Tanaka, H. (2000). "Seismic load test on interior and exterior beam-column joints with substandard reinforcing details", *ACI Structural Journal*, Vol. 97, No. 1, pp. 11–24.
- Hajime, O. and Kohichi, M. (1991). *Nonlinear Analysis and Constitutive Models of Reinforced Concrete*, Gihodo, Tokyo, Japan.
- Lehman, D. (2002). *Performance Characterisation of Non-ductile Reinforced Concrete Frame Components*, Pacific Earthquake Engineering Research (PEER) Report, Department of Civil and Environmental Engineering, University of Washington, Washington D.C., USA.
- RILEM 50-FMC Committee (1985). "Determination of the fracture energy of mortar and concrete by means of three-point bend tests on notched beams", *Materials and Structures*, Vol. 18, No. 4, pp. 287–290.
- Walker, S.G. (2001). *Seismic Performance of Existing Reinforced Concrete Beam–Column Joints*, Master Thesis, Department of Civil and Environmental Engineering, University of Washington, Washington D.C., USA.
- Wong, P.K.C., Priestley, M.J.N. and Park, R. (1990). "Seismic resistance of frames with vertically distributed longitudinal reinforcement in beams", *ACI Structural Journal*, Vol. 87, No. 4, pp. 488–498.

NOTATION

| | |
|----------------------------|---|
| A_i | area of intermediate reinforcement layer |
| A_s | area of tension reinforcement layer |
| A_g | gross area of section |
| b_j | effective joint width |
| c | cohesion |
| f'_c | concrete compressive stress |
| f_t | concrete tensile stress |
| G_F | fracture energy of concrete |
| h_c | column depth |
| N^* | axial compressive load |
| v_{jh} | nominal horizontal joint shear stress, $V_{jh}/h_c b_j$ |
| V_{jh} | maximum joint shear force |
| w_u | ultimate crack opening |
| ε_u^{cr} | ultimate strain in concrete |
| $\varepsilon_{uniaxial}^p$ | plastic strain in uniaxial stress direction |
| θ | angle of inclination of the diagonal compression strut |

